**Technical Issues**
**1/2016 pp. 82-89**
**ISSN 2392-3954**

# MECHANISM AND KINETICS OXIDATION OF INCONEL 617 AND 625 ALLOYS

**Katarzyna Staszewska**
**Mieczysław Scendo**
Uniwersytet Jana Kochanowskiego w Kielcach
Wydział Matematyczno–Przyrodniczy
Instytut Chemii
ul. Świętokrzyska 15G
25-406 Kielce
e-mail: katarzynastaszewska@onet.pl

**Abstract**: The mechanism and kinetics of oxidation of Inconel 617 and 625 alloys in air atmosphere were investigated. Materials were examined by the thermogravimetric method. The X-ray diffraction spectrometer (XRD) was used to observation change in chemical composition the oxide scales of Inconel alloys specimens. Oxidation kinetics was determined from weight-change measurements. The surface and microstructure of the sample were observed in an optical microscope (OM) and a scanning electron microscope (SEM). The results showed that the oxide scales of the alloys were compact and continuous. The layer were contained as the outer of $Cr_2O_3$, and the internal of $NiCr_2O_4$ spinel, NiO and other oxides. Oxides' scales with good adherence were formed on the surface of alloys. The kinetics and thermodynamic parameters of oxides formation were calculated and discussed for both alloys.

**Keywords:** Inconel alloys, Thermogravimetric analysis, Thermodynamic parameters, Parabolic rate constants, Activation energy.

## Introduction

Nickel – base alloys are available materials and in many cases stainless steel cannot prevent the corrosion attack [1]. The Inconel 617 and 625 alloys (superalloys) have good resistance to a wide variety of corrosive environments in industrial processes such as chemical and petrochemical processing. These alloys referring to their superior strength, adequate resistance to oxidation at elevated temperatures and retaining essentially a single-phase facecentered-cubic structure include a wide range of compositions based on nickel, chromium, cobalt, and molybdenum [2, 3]. The nickel content is sufficient for resistance to chloride ion stress corrosion cracking. The chromium improves resistance to high-temperature oxidation and to attack by hot sulphur-bearing gases. Moreover, chromium has a greater affinity for oxygen relative to other elements in the alloys and preferentially forms of Cr oxide, which gives an adherent stable and protective layer onto the alloy surface. The minor cobalt and molybdenum also aids resistance to pitting and crevice corrosion [4, 5].
This combination of elements is also responsible for superior resistance to a wide range of corrosive solutions of unusual severity as well as to high-temperature effects such as oxidation and carburization. However, oxidation at high temperature is much more aggressive and hence, spalling and internal oxidation occur even for short exposures and increase with time. Spalling occurs during cooling as a result of thermal stress and the main mechanism of oxidation in this case is cation diffusion. This provides a barrier to further oxidation surface of metal. The high-temperature corrosion occurs when components are in the high temperature and corrosion environments. This type of corrosion includes high-temperature oxidation, decarburizing, hydrogen corrosion, sulfidation corrosion and ablation [6]. The dependence of oxidation rates on temperature is well established and is known to obey an Arrhenius relationship.
The outstanding and versatile corrosion resistance of Inconel alloys under a wide range of temperatures and pressures is a primary reason for their wide acceptance in the chemical processing field. High tensile, creep, and excellent weldability and brazeability are the properties of Inconel alloys that make them interesting to the aerospace applications as aircraft ducting systems, engine exhaust systems, trust-reverser systems, hydraulic line tubing, and heat-exchanger tubing in environmental control systems.
The present paper concerns investigations on mechanism and kinetics of oxidation of Inconel 617 and 625 alloys. The samples were examined using a thermogravimetric method in air atmosphere. The chemical composition of the oxide scales were analysed by X – ray diffraction spectrometer (XRD). Oxidation kinetics was determined from weight-change measurements. The surface and microstructures were observed by an optical microscope (OM), and a scanning electron microscope (SEM).

## Experiment

### *Materials*

The materials of Inconel 617 and 625 were designed for the high-temperature oxidation in air atmosphere. Commercially available sheets of alloys were acquired from steel-works Forchungszentrum, Karlsruhre, Germany.

Table 1 presents the limiting chemical composition of both Inconel alloys.

High nickel, chromium, cobalt, and molybdenum contents (Table 1) make the alloys resistant to a variety of both reducing and oxidizing media. 617 and 625 alloys resist a wide range of severely corrosive environments and are especially resistant to pitting and crevice corrosion.

Tab. 1. Limiting chemical composition of alloys

| **Inconel 617** | **Ni** | **Cr** | **Co** | **Mo** | **Al** | **C** | **Fe** | **Ti** | **Cu** | **Mn** | **Si** | **S** |
|---|---|---|---|---|---|---|---|---|---|---|---|---|
| wt% | 44.5<br>61.7 | 20.0<br>24.0 | 10.0<br>15.0 | 8.0<br>10.0 | 0.80<br>1.50 | 0.05<br>0.15 | 3.00 | 0.60 | 0.50 | 1.00 | 1.00 | 0.015 |
| **Inconel 625** | **Ni** | **Cr** | **Mo** | **Nb** | **Fe** | **C** | **Mn** | **Si** | **Al** | **Ti** | **P** | **S** |
| wt% | 58.0<br>62.5 | 20.0<br>23.0 | 8.0<br>10.0 | 3.15<br>4.15 | 5.00 | 0.01 | 0.50 | 0.50 | 0.40 | 0.40 | 0.015 | 0.015 |

### *Thermogravimetric measurements*

Thermogravimetric measurements were carried out on a FCF2.0 CZYLOK muffle furnace. The samples for the testing were cut from the rolled new alloys bar and their dimensions were 6×6×6 mm. The geometric surface area of the samples was 2.16 $cm^2$. Before every measurement each specimen was carefully polished with emery 2500 grade paper. Then, the samples were rinsed with double distilled water, degreased with ethanol and were immediately immersed in the furnace. In order to eliminate the effects caused by the mass and heat transfer limitations, small quantities of samples (around 900 mg) were put into a $Al_2O_3$ crucible for each run under non-isothermal conditions.

The thermogravimetric baselines were corrected by subtraction of predetermined baselines which are determined under identical conditions except for the absence of a sample. The sample in the furnace was heated up from 100 to 1200 $^0$C (from 373 to 1473 K) the heating rate value was chosen according to planned temperature of measurements, Fig. 1.

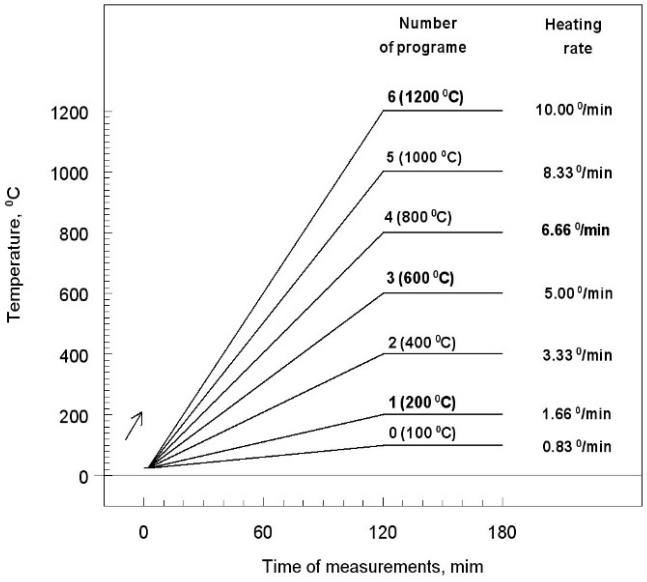


Fig. 1. Diagram temperature – time and heating rate of measurements.

For guaranteeing the air circulation and making samples be well-oxidized, during the measurement to interior cell of furnace was delivered the synthetic air with speed of 70 $cm^3$ $min^{-1}$.
The changes of mass of samples were controlled for every temperature of measurement. The sensitivity of the balance was $1\times10^{-5}$ g.

***Kinetic studies***
Kinetic studies, based on the change of mass were obtained by the thermogravimetric curves analysis [7-13]. The oxidation process can be expressed as:

$$\left(\frac{\Delta m}{S}\right)^n = k_p t \quad (1)$$

where $\Delta m$ and S are the sample weight and surface area, $n$ is the exponential term, $k_p$ is the oxidation rate constant, and $t$ is the oxidation time. The oxidation rate of materials at the high temperature can be estimated by the increase in scale thickness ($X_{scale}$), with time:

$$\beta_{scale} = \frac{d\,X_{scale}}{d\,t} \quad (2)$$

The activation energy for the oxidation process was calculated on the basis the Arrhenius type plot according to the equation:

$$k_p = A\exp\left(-\frac{E_a}{RT}\right) \quad (3)$$

or:

$$E_a = -RT\ln\left(\frac{k_p}{A}\right) \quad (4)$$

where $A$ is the Arrhenius pre-exponential constant, $E_a$ is the activation energy, $R$ is the universal gas constant, and $T$ is the absolute temperature. However, in the coordinate system of ln $k_p$ vs. $1/T$ a straight line whose slope allows an evaluation of the activation energy was obtained.

***Additional measuring instruments***
The radiation source of the X-ray diffractometer (XRD) was CuKα with Ni filter and generated at 1.2 kW with scan rate 0.25 $^0$/s was used to determine the chemical composition of oxide scales. The surface of the samples was observed in an optical microscope (OM). The cross-section of microstructure was investigated by a scanning electron microscope (SEM), Joel, type JSM-5400. The accelerating voltage was 20 kV. Each test was repeated four times to verify the reproducibility of data and the average values were reported.

## Results

***Thermogravimetric measurements***
The change mass of Inconel 617 in referring to the temperature for different times exposition of samples in air atmosphere is presented in Fig. 2. However, the similar results were received for Inconel 625 alloy.

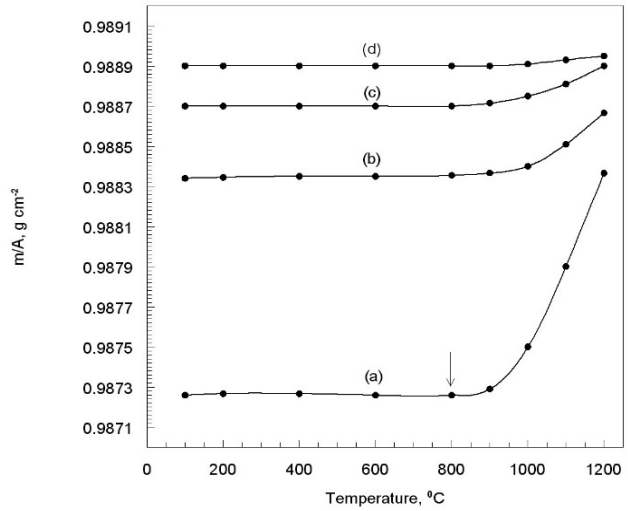


Fig. 2. Change mass of Inconel 617 in referring to the temperature for times exposition: (a) 24, (b) 48, (c) 72, and (d) 96 hours. Arrow was a mark of critical temperature conversion.

The weight gain of samples was observed after the achievement of the critical temperature conversion in which the increase of the mass of a sample achieved the value of 1% in relation to the mass of the initial specimen, Table 2.

Tab. 2. Critical temperature conversion, weight gain of Inconel alloys in air atmosphere.

| Inconel alloy | Critical temperature conversion $^0$C | Weight gainsample mg |
|---|---|---|
| 617 | 803 | 0.0110 |
| 625 | 767 | 0.0128 |

The thermogravimetric experiments in air atmosphere demonstrated that in the first period, the oxide scale on the surface of alloys was very thin so that the oxygen atoms diffuse easily through it and the oxidation reacts quickly (Fig. 2, curve (a)). With time, the oxide scales became more continuous and compact which reduced further the diffusion rate of oxygen atoms and limited the oxidation reaction (Fig. 2, curves (b)-(d)). The optical micrograph of surface of Inconel 617 and 625 alloys after thermogravimetric measurements were presented in Fig. 3.

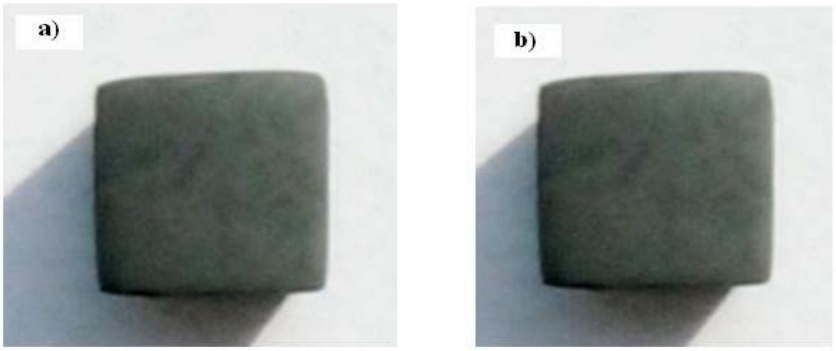


Fig. 3. Optical micrograph of surface of Inconel: a) 617 and b) 625 after thermogravimetric measurements. Magnification 20×.

The oxides' scales with good adherence were formed on the surface of both Inconel alloys, and performed excellent high-temperature oxidation resistance.

***Ellingham diagram***

The Ellingham diagram is essentially a graph representing the thermodynamic driving force for a particular reaction to occur, across a range of temperatures. The diagram plots represent the standard free energy ($\Delta G^0 = -RT \ln p\,O_2$) change of a reaction as a function of temperature. The free energy change of a chemical reaction is the difference in free energy between the products of the reaction and the reactants. A chemical reaction will occur if the total free energy of the products is less than total free energy of the reactants. If the system coating the reactants and products is closed, the concentration of reactants will decrease and the concentration of products will increase as the reaction proceeds [14]. Fig. 4 shows the Ellingham diagram for formation of oxides of niobium, chromium, molybdenum, cobalt, and nickel.

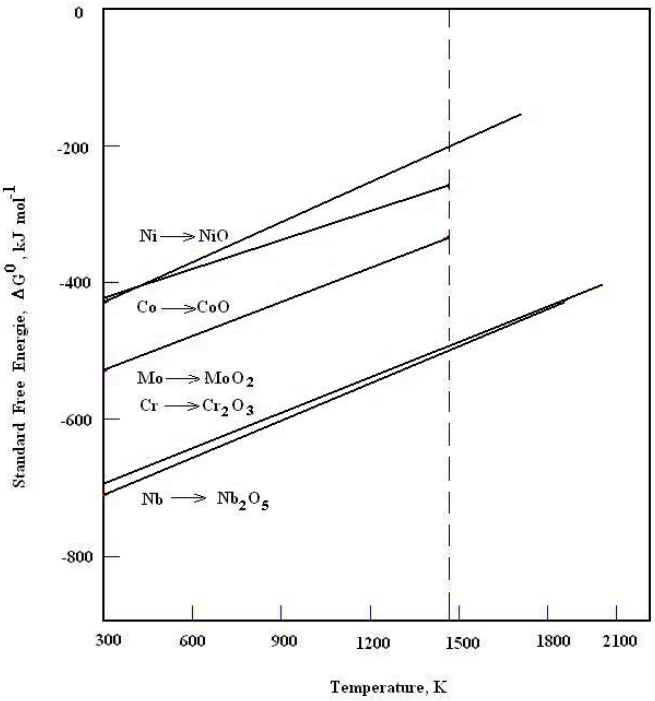


Fig. 4. Ellingham diagram for formation reactions of oxides of chosen metals.

Negative values for $\Delta G^0$ show that formation oxides of $Nb_2O_5$, $Cr_2O_3$, $MoO_2$, CoO and NiO proceed spontaneously without external inputs. The standard free energy change is greater (more negative) for the niobium oxidation relative to that of molybdenum, cobalt, and nickel at all temperatures. This means that at all temperatures the equilibrium constant is larger for the niobium reaction, therefore the composition is further weighted towards the products of the reaction. This is the reason why metals that appear higher up on the diagram (Ni) are more stable than those metals that appear lower down (Nb or Cr) and are more likely to be found in their pure oxides solid form. Moreover, the free energy change for niobium or chromium oxidation reaction is much lower than for nickel oxidation reaction, what means that Nb is more oxidative than Ni. By using the diagram (Fig. 4) the standard free energy change for formation reactions of oxides of Nb, Cr, Mo, Co and Ni can be found at 1473 K. The values of equilibrium constant and $\Delta G^0$ were listed in Table 3.

Tab. 3. Formation reaction of oxides, equilibrium constants, equation plots, and standard free energy change at 1473 K.

| **Reaction** | **Equilibrium constant** | **Equation plot** | **$\Delta G^0$ kJ mol$^{-1}$** |
|---|---|---|---|
| $Nb \rightarrow Nb_2O_5$ | $1.06 \times 10^{18}$ | *-755 + 0.17 T* | -508 |
| $Cr \rightarrow Cr_2O_3$ | $4.34 \times 10^{17}$ | *-740 + 0.16 T* | -497 |
| $Mo \rightarrow MoO_2$ | $6.46 \times 10^{11}$ | *-578 + 0.17 T* | -333 |
| $Co \rightarrow CoO$ | $1.59 \times 10^{9}$ | *-491 + 0.16 T* | -259 |
| $Ni \rightarrow NiO$ | $5.26 \times 10^{7}$ | *-471 + 0.17 T* | -218 |

The oxidation mechanism of metal at the high-temperature and in the air atmosphere condition usually depends from (i) the transport of oxidant gas from the bulk gas phase, (ii) phase boundary reactions at the gas/scale interface, or (iii) the diffusion of metal cations to the scale/gas phase interface. The oxidation of metal at the high-temperature conditions should be considered as electrochemical process. Therefore, in the case of Inconel alloys the process of forming an oxide layer on the surface of the clean metal begins from the adsorption of oxygen by Cr atoms:

$$2\ Cr + 3/2\ O_{2(g)} \rightarrow Cr_2O_{3(S)}. \quad (5)$$

The $Cr_2O_3$ layer was quickly formed on the surface of alloy. In case of Inconel 625, the layer of $Cr_2O_3$ was replenished by oxide of niobium:

$$2\ Nb + 5/2\ O_{2(g)} \rightarrow Nb_2O_{5(S)}. \quad (5a)$$

Then the layer of oxides on the surface of metal carries out the part as specific solid electrolyte.

The outside surface of oxide layer behaves as:

Cathode:

$$O_{2(g)} + 4\ e^- \rightarrow 2\ O^{2-}. \quad (6)$$

On the other hand, the surface of the metal performs the role:

Anode:

$$2\ Ni + 2\ O^{2-} - 4\ e^- \rightarrow 2\ NiO_{(S)}. \quad (7)$$

The $Cr_2O_3$ particles were surrounded with NiO and the solid-state reaction occurred to form spinel according to the chemical reaction:

$$Cr_2O_3 + NiO \rightarrow NiCr_2O_{4(S)}. \quad (8)$$

Moreover, the $NiCr_2O_4$ spinel can also reduce the diffusion velocity of metal ion, which decreases the bonded rate of the metal ion and oxygen atom. The oxidation resistance of the alloys will be enhanced. When the oxidation reaction enters the second oxidation stage:

$$Mo + 2\ O^{2-} - 4\ e^- \rightarrow MoO_{2(S)}. \quad (9)$$

However, over layer surface of material native of Inconel 617 appeared:

$$Co + O^{2-} - 2\ e^- \rightarrow CoO_{(S)}. \quad (10)$$

Therefore, the continuous and compact of oxide scales were improved considerably.

***Oxidation kinetics***

Oxidation kinetic curves of Inconel 617 and 625 alloys in the air atmosphere at 1473 K for 96 hours exposition were shown in Fig. 5.

The oxidation of Inconel alloys at high-temperature can be classified into two stages: (i) An initial stage characterized by a linear type oxidation, about 24 hours exposition in the case both of alloys (Fig. 5), (ii) The final stage oxidation of metals where a transition from linear to parabolic mechanism takes place [15], Fig. 6.

Fig. 6 illustrates parabolic reaction rate behavior of Inconel 617 and 625, which can be divided into two periods. In the first period the oxidation are linear with testing time. The oxide layers reached a thickness after which the oxidation process became controlled by the solid state diffusion of the oxidizing species through the scale layers. Therefore, the oxide scales are very thin and not continuous in some positions so that the oxygen atoms diffuse easily through them and the oxidation reacts quickly. However, in the second period, the rates of oxidation show a slight decrease and were followed according to parabolic rate laws. In this case oxidation of alloys were independent of furnace atmosphere composition. The adherence of oxide scales prevents effectively the diffusion from the environment and the alloys exhibit excellent high-temperature oxidation

resistance. This diffusion controlled process is known as parabolic oxidation where the parabolic rate constants ($k_p$) are expressed by Equation (1). Moreover, the exponential term $n$ represents the type of oxidation mechanism. In this case $n$ = 2, therefore the oxidation process is parabolic for both alloys.

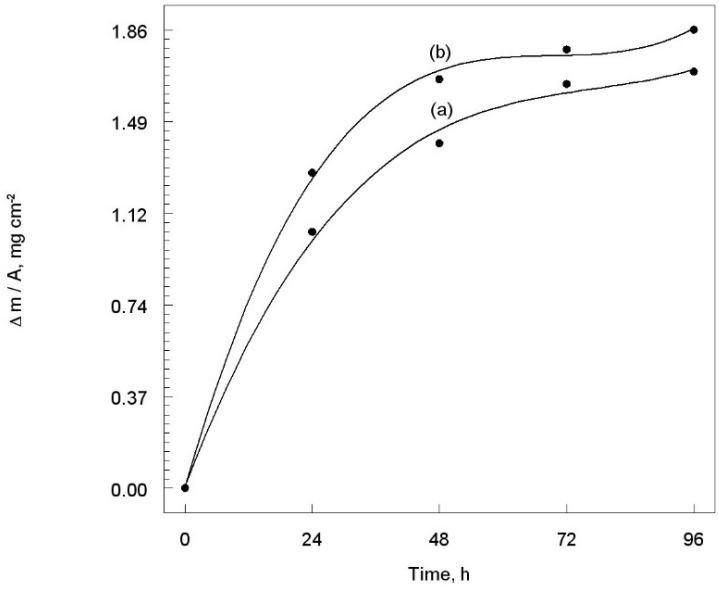


Fig. 5. Oxidation kinetic curves of Inconel: (a) 617 and (b) 625 at 1473 K for 96 hours exposition.

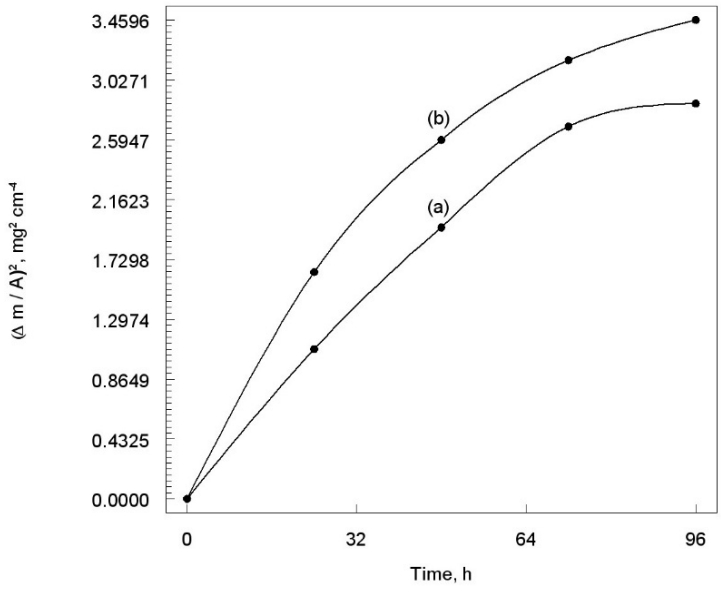


Fig. 6. Parabolic characteristic of Inconel: (a) 617 and (b) 625 oxidation kinetics.

The rates of oxidation of Inconel 617 and 625 alloys can be best compared by looking at their oxidation rate constants, which can be obtained from the analysis of the weight gain data during oxidation of alloys and are given in Table 4.

The parabolic rate constants over the temperature range from 1273 to 1473 K for the Inconel 617 and 625, respectively and can be expressed as:

$$k_p = 1.93\times10^{-9}\,T + 5.94\times10^{-6} \quad (11)$$

and:

$$k_p = 1.07\times10^{-9}\,T + 8.73\times10^{-6} \quad (12)$$

However, the parabolic rate constant for Inconel 617 is about 2 times smaller in comparison to Inconel 625 alloy.

Tab. 4. Temperature, and parabolic rate constants for oxidation of Inconel alloys in air atmosphere.

| Inconel alloy | Temperature K | $k_p$ $mg^2/cm^4s$ |
|---|---|---|
| 617 | 1273 | $7.88 \times 10^{-6}$ |
| | 1373 | $8.07 \times 10^{-6}$ |
| | 1473 | $8.26 \times 10^{-6}$ |
| 625 | 1273 | $9.79 \times 10^{-6}$ |
| | 1373 | $9.90 \times 10^{-6}$ |
| | 1473 | $1.00 \times 10^{-5}$ |

***Activation energy***

Activation energy ($E_a$) may be defined as the minimum energy required to start a chemical reaction. Moreover, $E_a$ can be thought as the height of the energy barrier separating two minima of potential energy of the reactants and products of a reaction.

According to Equations (3) or (4) a plot of ln $k_p$ against $1/T$ should be a straight line. Fig. 7 presents the Arrhenius plots for the Inconel 617 and 625 alloys.

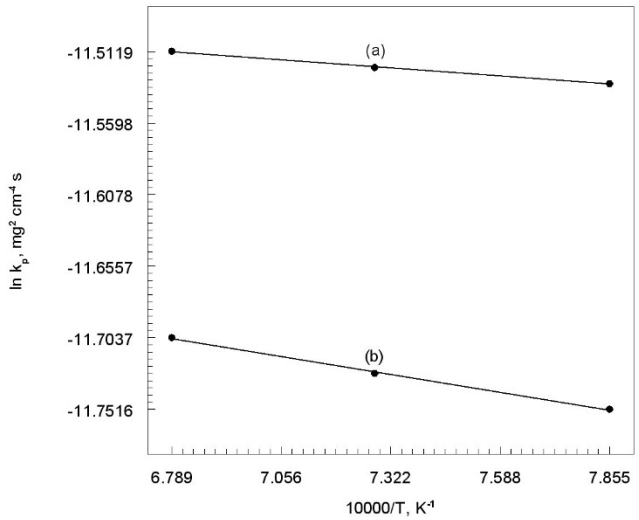


Fig. 7. Arrhenius plots for oxidation of Inconel: (a) 617 and (b) 625.

The linear correlation coefficients ($R^2 > 0.999$) were good for linear plots. Therefore, the slope of the line can be used to estimate the activation energy ($E_a$) of the oxidation process of the materials.

However, the linear correlation coefficients and the activation energy are given in Table 5.

Tab. 5. Linear correlation coefficients and activation energy of Inconel alloys in air atmosphere.

| Inconel alloy | $R^2$ | $E_a$ kJ / mol |
|---|---|---|
| 617 | 0.9999 | 374 |
| 625 | 1.0000 | 168 |

For oxidation of the Inconel 617 the activation energy was found to be 374 kJ/mol, and that for oxidation of the Inconel 625 alloy was 168 kJ/mol, both indicative of a parabolic rate type of oxidation mechanism. Therefore, the minimum energy was required to start oxidation of the Inconel 625 alloy.

## Conclusions

Considering overall experimental results, the following conclusions can be drawn:
1 - After exposure of Inconel 617 and 625 alloys in air atmosphere at high temperature the external oxide layer of the alloys consisted of $Nb_2O_5$ (Inconel 625 only) $Cr_2O_3$, and the internal oxide layer were of $NiCr_2O_4$ spinel, $MoO_2$, CoO (Inconel 617 only) or NiO oxides;
2 - The oxidation mechanism of the alloys was that the external oxidation and internal oxidation were formed simultaneously;
3 - The oxidation of both alloys was controlled by the transmission of metal and oxygen ions through the oxide scales. The oxide scales growth depends on the diffusion of reagents;
4 - The adherence of oxide scales prevents effectively the oxygen diffusion from the environment;
5 - The oxidation kinetic behavior of Inconel 617 and 625 alloys obeyed the parabolic laws;
6 - The Inconel 617 alloy exhibits excellent high-temperature oxidation resistance.

## REFERENCES

1. Siddique, M., Hussain, N., Shafi, M., Identification of Iron Oxides Qualitatively/Quantitatively Formed during the High Temperature Oxidation of Superalloys in Air and Steam Environments, *J. Mater. Sci. Technol*., 2009, 25, pp. 479-482.
2. Kawakita, J., Kuroda, S., Fukushima, T., Kodama, T., Corrosion resistance of HVOF sprayed HastelloyC Nikel base Allom In seawater, *Corros. Sci.*, 2003, 45, pp. 2819-2835.
3. Thomas, A., El-Wahabi, M., Cabrera, J.M., Prado, J.M., High temperature deformation of Inconel 718, *J. Mater. Process. Technol*., 2006, 177, pp. 469-472.
4. Liu, L., Li, Y., Wang, F.H., Influence of micro-structure on corrosion behavior of a Ni-based superalloy in 3.5% NaCl, *Electrochim. Acta.*, 2007, 52, pp. 7193-7202.
5. Yin, Z.F., Ahao, W.Z., Lai, W.Y., Zhao, X.H., Electrochemical behaviour of Ni-base alloys exposed under oil/gas field environments, *Corros. Sci*., 51, pp. 1702-1706.
6. Tawancy, H.M., Sridhar, N., High-Temperature Oxidation behavior of a Ni-Cr-Al-Fe-Y a Alloy, *Oxid. Met*. 1992, 37, pp. 143-166.
7. Zuru, A.A., Dangoggo, S.M., Birnin-Yauri, U.A., Tambuwal, A.D., Adoption of thermogravimetric kinetic models for kinetic analysis of biogas production, *Renew. Energy*, 2004, 29, pp. 97-107.
8. Xiao, H.M., Ma, X.Q., Li, Z.Y., Isoconversional kinetic analysis of co-combustion of sewage sludge with straw and coal, *Appl. Energy*, 2009, 86, pp. 1741-1745.
9. Bouklah, M., Attayibat, A., Kertit, S., Ramdani, A., Hammouti, B., A pyrazine derivative as corrosion inhibitor for steel in sulphuric acid solution, *Appl. Surf. Sci*., 2005, 242, pp. 399-406.
10. Bouklah, M., Hammouti, B., Lagrenée, M., Bentiss, F., Thermodynamic properties of 2,5-bis(4-methoxyphenyl)-1,3,4-oxadiazole as a corrosion inhibitor for mild steel in normal sulfuric acid medium, *Corros. Sci*., 2006, 48, pp. 2831-2842.
11. Scendo, M., 2005. Potassium ethyl xanthate as corrosion inhibitor for copper in acidic chloride solutions, *Corros. Sci*., 2005, 47, pp. 1738-1749.
12. Scendo, M., Corrosion inhibition of copper by potassium ethyl xanthate in acidic chloride solutions, *Corros. Sci*., 2005, 47, pp. 2778-2791.
13. Scendo, M., Trela, J., Radek, N., Purine as an Effective Corrosion Inhibitor for Stainless Steel in Chloride Acid Solutions, *Corros. Rev*., 2012, 30, pp. 33-45.
14. Atkins, P., Julio, P., Physical Chemistry: Thermodynamics and Kinetics (8th ed.). W.H. Freeman, 2006.
15. Pavithra, M.K., Venkatesha, T.V., Punith Kumar, M.K., Tondan, H.C., 2012. Inhibition of mild steel corrosion by Rabeprazole sulfide, *Corros. Sci*., 2012, 60, pp. 104-111.

*This research was supported by "The National Centre of Research and Development", a project of Technologies of Laser Welding for Energetic and the Protection of Environment (No. PBS1/B5/13/2012). The research part of the project of "1.3. Investigation of corrosive resistance of joints in the high-temperature conditions" was realized in the Institute of Chemistry, Jan Kochanowski University in Kielce.*